Molecular Biology of the Cell
Vol. 16, 5686–5698, December 2005

Zonula Occludens-1 Alters Connexin43 Gap Junction Size and Organization by Influencing Channel Accretion

Andrew W. Hunter, Ralph J. Barker, Ching Zhu, and Robert G. Gourdie

Department of Cell Biology and Anatomy, Cardiovascular Developmental Biology Center, Medical University of South Carolina, Charleston, SC 29425

Submitted August 9, 2005; Revised September 13, 2005; Accepted September 15, 2005
Monitoring Editor: Asma Nusrat

Regulation of gap junction (GJ) organization is critical for proper function of excitable tissues such as heart and brain, yet mechanisms that govern the dynamic patterning of GJs remain poorly defined. Here, we show that zonula occludens (ZO)-1 localizes preferentially to the periphery of connexin43 (Cx43) GJ plaques. Blockade of the PDS95/dlg/ZO-1 (PDZ)-mediated interaction between ZO-1 and Cx43, by genetic tagging of Cx43 or by a membrane-permeable peptide inhibitor that contains the Cx43 PDZ-binding domain, led to a reduction of peripherally associated ZO-1 accompanied by a significant increase in plaque size. Biochemical data indicate that the size increase was due to unregulated accumulation of gap junctional channels from nonjunctional pools, rather than to increased protein expression or decreased turnover. Coexpression of native Cx43 fully rescued the aberrant tagged-connexin phenotype, but only if channels were composed predominately of untagged connexin. Confocal image analysis revealed that, subsequent to GJ nucleation, ZO-1 association with Cx43 GJs is independent of plaque size. We propose that ZO-1 controls the rate of Cx43 channel accretion at GJ peripheries, which, in conjunction with the rate of GJ turnover, regulates GJ size and distribution.

INTRODUCTION

The gap junction (GJ) is a plaque-like aggregate of intercellular channels that facilitates cytoplasmic interchange of ions, second messengers, and other molecules <1 kDa between cells (Goodenough *et al*., 1996). Frequent and variably sized GJ channel aggregates couple most cells in animal tissues. In excitable organs such as the heart and brain, GJs show distinctive organizational patterns that configure extended intercellular pathways for stable and long-term propagation of action potential (Lo, 2000). The channels comprising individual GJ plaques are composed of proteins encoded by the connexin family of genes (Willecke *et al*., 2002). Assembly of GJs from connexin monomers is thought to proceed in a multistep process (Musil and Goodenough, 1991, 1993). First, six connexins oligomerize into a hemichannel, called a connexon, followed by trafficking to the plasma membrane. Subsequently, a connexon docks with a second connexon from the apposed membrane of an adjacent cell to form an intercellular channel. In a process that occurs either simultaneous with or after this docking step, channels aggregate to form the functional organelle of cell-cell communication—the GJ plaque.

The gating of single channels within a GJ plaque is regulated by various stimuli, including voltage, pH, and phosphorylation (Saez *et al*., 2003). Intercellular communication is also regulated at the level of the plaque as a whole by factors that affect the abundance, size, and cellular distribution of GJ channel aggregates (Hall and Gourdie, 1995; Bukauskas *et al*., 2000; Spach *et al*., 2000; Johnson *et al*., 2002; Lauf *et al*., 2002). Irregularities in the extent and geometry of gap junctional contacts have been implicated in cardiac and neural electrophysiological pathologies in humans, including ischemic heart disease (Smith *et al*., 1991), hypertrophic cardiomyopathy (Sepp *et al*., 1996), heart failure (Dupont *et al*., 2001), and medial temporal lobe epilepsy (Fonseca *et al*., 2002). At present, the mechanisms governing higher order aspects of GJ organization and function in health and disease are poorly understood.

Nonetheless, there is a growing understanding that an array of proteins interact with connexins, potentially mediating linkage of GJs to other junction types, signal transduction molecules, and the cytoskeleton (Giepmans, 2004). One connexin-interacting molecule that has received particular attention is zonula occludens (ZO)-1. Originally discovered in association with tight junctions (Stevenson *et al*., 1986), ZO-1 is a member of the membrane-associated guanylate kinase (MAGUK) family of proteins that function in protein targeting, signal transduction, and determination of cell polarity (Anderson, 1996). MAGUKs, such as ZO-1, synaptic protein PSD95, and the *Drosophila* tumor suppressor discs large (dlg), are characterized by an N-terminal array of protein-binding domains that includes one or more PDS95/dlg/ZO-1 (PDZ) domains. Previous immunoprecipitation and yeast two-hybrid studies showed that a short PDZ-binding motif at the C terminus of connexin43 (Cx43) interacts with the second of three PDZ domains in ZO-1 (Giepmans and Moolenaar, 1998; Toyofuku *et al*., 1998). Subsequently, other connexins have been reported to interact with ZO-1 via a consensus C-terminal PDZ-binding domain similar to that of Cx43 (Jin *et al*., 2000; Kausalya *et al*., 2001; Laing *et al*., 2001; Nielsen *et al*., 2003; Li *et al*., 2004).

Initially, ZO-1 function at GJs was assumed to be analogous to its presumed role at tight junctions. Namely, ZO-1

This article was published online ahead of print in *MBC in Press* (http://www.molbiolcell.org/cgi/doi/10.1091/mbc.E05–08–0737) on September 29, 2005.

Address correspondence to: Andrew W. Hunter (huntera@musc.edu) or Robert G. Gourdie (gourdier@musc.edu).

Abbreviations used: AJ, adherens junction; Cx43, connexin43; GJ, gap junction; MOI, multiplicity of infection; PDZ, PDS95/dlg/ZO-1; ZO, zonula occludens.

was envisaged as a passive scaffolding molecule that stabilizes GJs through cytoskeletal anchoring. However, subsequent reports have indicated that interactions between connexins and ZO-1 may encompass other, more dynamic functions. In particular, changes in Cx43–ZO-1 interaction have been noted during remodeling of GJs in cardiomyocytes and other cell types (Defamie *et al*., 2001; Barker *et al*., 2002; Segretain *et al*., 2004). Moderation of Cx43–ZO-1 interaction by c-Src has lead others to hypothesize a role for ZO-1 in the regulation of GJ channel activity (Giepmans *et al*., 2001a; Toyofuku *et al*., 2001; Duffy *et al*., 2004; Sorgen *et al*., 2004). As such, definitive roles for ZO-1 interaction with connexins remain to be determined. Here, we provide evidence that ZO-1 regulates the cellular distribution of Cx43, and consequently the size of GJ plaques, by controlling the rate of channel accretion at plaque perimeters.

MATERIALS AND METHODS

Animals

Hearts were harvested from 2- to 3-d-old Holtzman Sprague Dawley rats. Animal care was in accordance with institutional guidelines at the Medical University of South Carolina, Charleston, SC (Animal welfare assurance #A4328-01).

Antennapedia Peptides

Antennapedia peptides (Lindgren *et al*., 2000) were generated at Medical University of South Carolina or by Research Genetics (Huntsville, AL). The inhibitor peptide includes the Cx43 C-terminal amino acids 374–382 (RPRPDDLEI) that encompass the ZO-1-binding sequence. A control peptide was generated by reversing the Cx43 amino acid sequence (IELDDPRPR). Both peptides contain a 16-amino acid antennapedia internalization vector (RQPKIWFPNRRKPWKK) linked to the N terminus of the Cx43 (or reversed Cx43) sequence; peptides were N-terminally biotinylated.

Cell Culture

Neonatal cardiomyocytes were isolated with a Neonatal Cardiomyocyte Isolation System (LK003300; Worthington Biochemicals, Freehold, NJ) according to manufacturer's instructions. Cultures were generated from 8 to 12 hearts. Dispersed cardiomyocytes were plated on coverglass or culture dishes coated with 0.2% gelatin (Sigma-Aldrich, St. Louis, MO). Cytosine arabinoside (Sigma-Aldrich) was used to inhibit fibroblast proliferation. Cardiomyocytes were cultured as described previously (Barker *et al*., 2002) as monolayers for 72 h before peptide treatments.

HeLa cells stably expressing either native Cx43 or Cx43-EGFP (Jordan *et al*., 1999) were cultured as described previously (Hunter *et al*., 2003) for 24–48 h before peptide treatments or adenoviral infection. Newly confluent cultures were used for all experiments.

Adenovirus expressing human Cx43 (Qbiogene, Carlsbad, CA) was added to cells (at various multiplicities of infection [MOIs]) in Opti-MEM and allowed to adsorb for several hours before addition of culture medium. Adenoviral expression progressed for 24 h subsequent to further manipulations.

Peptides were added to cells at 30 μM, which falls within the effective range (1–100 μM) for antennapedia peptides (Lindgren *et al*., 2000). Media containing peptides were replenished every 24 h.

Determination of Connexin Expression Levels, Stoichiometry, and Turnover

Cx43 expression was assessed in cardiomyocytes and HeLa Cx43 cells cultured for 48 and 72 h, respectively, with or without peptides. Cells were solubilized in hot 4% SDS sample buffer for 5 min, sheared, and boiled for 5 min. Samples were resolved by 10% SDS-PAGE and immunoblotted with Cx43 (71-0700; Zymed Laboratories, South San Francisco, CA) and glyceraldehyde-3-phosphate dehydrogenase (GAPDH) (Research Diagnostics, Flanders, NJ) antibodies. Sample loading was normalized to GAPDH signal.

To determine stoichiometry and turnover in connexin-expressing HeLa cells, metabolic labeling with [^{35}S]methionine (35–100 μCi/ml; PerkinElmer Life and Analytical Sciences, Boston, MA), pulse-chase analysis, and immunoprecipitations using Cx43 antibodies (C6219; Sigma-Aldrich) were performed as described previously (VanSlyke and Musil, 2000). Immunoprecipitated Cx43 and Cx43-GFP were resolved by 10% SDS-PAGE. Dried gels were exposed to phosphor screens; ^{35}S-labeled connexins were detected using a Storm PhosphorImager and quantified using ImageQuant (Molecular Dynamics, Sunnyvale, CA). Curve fitting of pulse-chase data were performed with IGOR Pro (Wavemetrics, Lake Oswego, OR).

Pull-Down Assays

Glutathione *S*-transferase (GST)-fusion proteins composed of either the PDZ1 (amino acids 1–106) or PDZ2 (amino acids 173–261) domain of human ZO-1 were generated as described previously (Nielsen *et al*., 2002) and isolated from isopropyl β-D-thiogalactoside-induced DH5α bacteria according to standard procedures.

HeLa Cx43 cells were lysed in 50 mM Tris-HCl, pH 7.4, 150 mM NaCl, 2 mM EGTA, 1% NP-40, 0.25% Na-deoxycholate, 100 μM phenylmethylsulfonyl fluoride (PMSF), and 1× Complete protease inhibitors (Roche Diagnostics, Indianapolis, IN) for 30 min at 4°C and then centrifuged at 16,000 × *g* for 10 min at 4°C. Fusion proteins (2–3 μg) coupled to glutathione-Sepharose 4B beads (GE healthcare, Little Chalfont, Buckinghamshire, United Kingdom) were added to clarified lysates containing peptides (100 μM). Reactions were incubated sequentially with GST-PDZ1 and GST-PDZ2 beads, each for 1 h at 4°C. Pelleted beads were washed three times with lysis buffer. Pelleted material was resolved by 10% (Cx43) and 10–20% (peptides) SDS-PAGE. Western blot detection was performed with streptavidin-horseradish peroxidase (HRP) (GE Healthcare) and Cx43 antibodies (C6219; Sigma-Aldrich).

Triton X-100 Fractionation Assay

Peptide-treated HeLa Cx43 cells were lysed in 1% Triton X-100 in phosphate-buffered saline (PBS) plus 100 μM PMSF and 1× Complete protease inhibitors for 1 h on ice with occasional vortexing and then centrifuged at 10,000 × *g* for 5 min at 4°C. Triton-soluble fractions (supernatants) were removed, and Triton-insoluble fractions (pellets) were resuspended in an equal volume of lysis buffer. Equal volumes of Triton-soluble and -insoluble fractions were resolved by 10% SDS-PAGE and immunoblotted with Cx43 antibody (71-0700; Zymed Laboratories). Signal was detected by alkaline phosphatase-based chemiluminescence (CDP-Star; Tropix, Bedford, MA) exposed to Hyperfilm ECL (GE Healthcare). Blots were digitized using a UMAX PowerLook scanner and VueScan (Hamrick Software, Phoenix, AZ). Quantitative densitometry was performed with ImageJ (National Institutes of Health; http://rsb.info.nih.gov/ij/); soluble/insoluble ratios were calculated from area-underpeak measurements; insoluble Cx43 isoform ratios were calculated from peak height measurements.

Fluorescence Labeling

Cells grown on coverglass were fixed in 2% paraformaldehyde in PBS for 10 min, blocked with 1% bovine serum albumin, 0.1% Triton X-100 in PBS, and immunolabeled with Cx43 (610062; BD Transduction Laboratories, Lexington, KY; MAB3067; Chemicon International, Temecula, CA) and ZO-1 (61-7300; Zymed Laboratories) antibodies. Signal was detected directly by green fluorescent protein (GFP) fluorescence or by secondary antibodies conjugated with Alexa488, Alexa546 (Invitrogen, Carlsbad, CA), or Cy5 (Jackson ImmunoResearch Laboratories, West Grove, PA). Biotinylated peptides were detected using streptavidin-Cy5 (Jackson ImmunoResearch Laboratories). To delineate plasma membrane, tetramethylrhodamine B isothiocyanate-wheat germ agglutinin (TRITC-WGA) (Sigma-Aldrich) was added (5 μg/ml) to live HeLa Cx43 cultures for 5 min before fixation. Samples were mounted in SlowFade (Invitrogen).

Confocal Microscopy

Optical sections were captured with a TCS SP2 AOBS laser scanning confocal microscope equipped with a 63×/1.4 numerical aperture oil immersion objective (Leica Microsystems, Deerfield, IL). Lasers used were Ar (488 nm), Kr (568 nm), and HeNe (633 nm). Pinhole (=airy disk), gain, and black level settings were held constant. Potential overlaps in emission spectra were eliminated by sequential scanning and tuning of the AOBS. For quantitative analyses of single optical sections, scan format and zoom were adjusted to give *x*-*y* pixel sizes of 68 × 68 nm for myocyte images and 116 × 116 nm for HeLa cell images. Maximum projections were generated from *z*-series with *x*-*y*-*z* voxel dimensions of 68 × 68 × 400–730 nm for myocyte images and 124 × 124 × 124 nm for HeLa cell images.

Image Analysis

GJ lengths, GJ number, total Cx43 area, and individual plaque areas were measured from single optical sections as described previously (Green *et al*., 1993; Hunter *et al*., 2003). HeLa cell analysis was modified by limiting measurements to Cx43 signal colocalized with TRITC-WGA signal at cell–cell borders. Parameter means were calculated from image averages, except in the case of GJ mean lengths and size distributions, which were determined from the entire sampled populations. Quantification of ZO-1 colocalization with individual Cx43 plaques was carried out according to Zhu *et al*. (2005). Linear regression analysis of Cx43–ZO-1 colocalization was performed in IGOR Pro.

Statistics

Multiple data sets were compared using analysis of variance ($p > 0.05$ rejected as not significant) and unpaired, two-tailed Bonferroni *t* tests ($p > 0.05/3 \approx 0.017$ rejected as not significant). Size distributions were compared using nonparametric chi-square and Mann-Whitney rank sum tests. Where

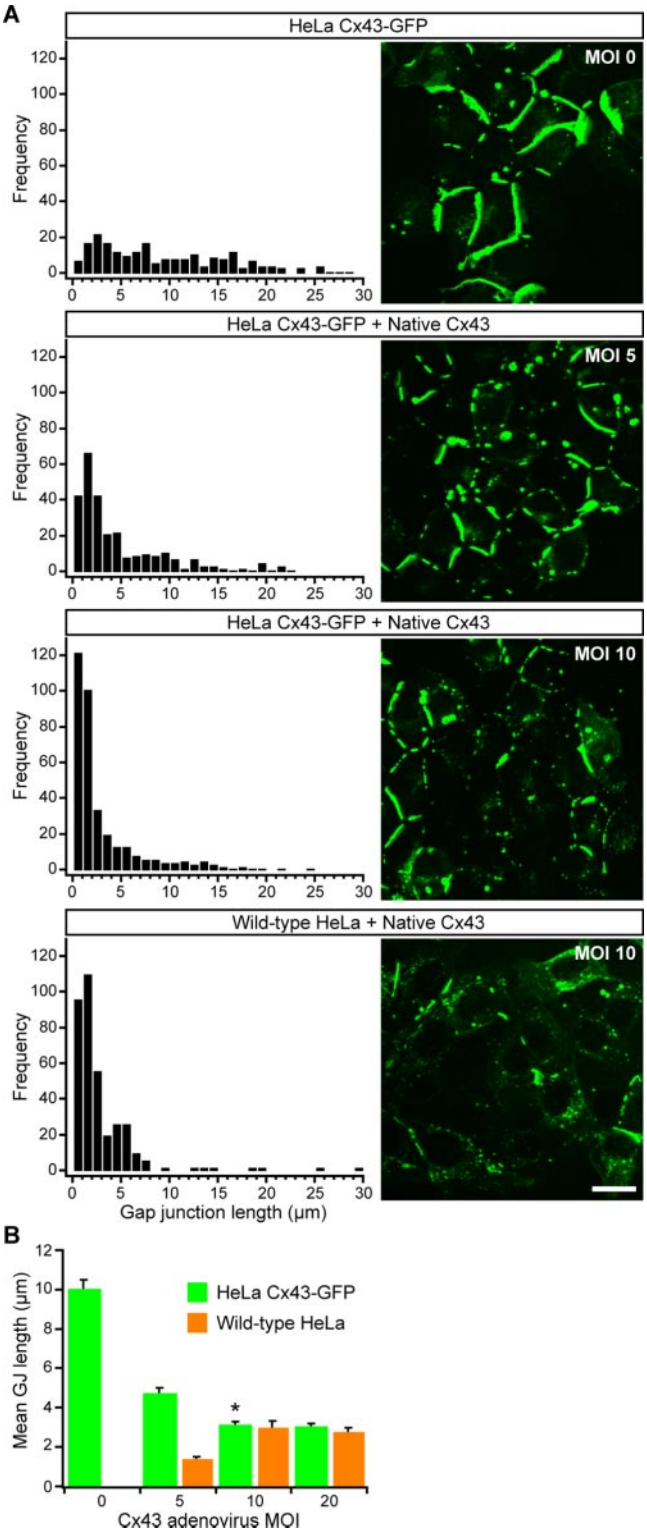

Figure 1. Coexpression of native Cx43 in HeLa Cx43-GFP cells normalizes gap junction size and distribution. (A) Confocal optical sections of GFP fluorescence in HeLa Cx43-GFP cells coexpressing increasing levels of native Cx43 (i.e., increasing viral MOI) and corresponding length distributions generated from measurements of membrane-localized Cx43-GFP plaques. Bottom, length distribution of Cx43 GJs after viral expression of native Cx43 at MOI 10 in wild-type HeLa cells. Bar, 20 μm. (B) Mean length of Cx43-GFP GJs as a function of native Cx43 viral expression (mean ± SE). Coexpression of native Cx43 at MOI 10 resulted in a >3-fold reduction in the mean length of mixed GJs relative to pure Cx43-GFP GJs (MOI 0). Asterisk (*) indicates that the GJ size distribution in HeLa Cx43-GFP cells expressing native Cx43 at MOI 10 was significantly different ($p < 0.001$) from the GJ distribution in HeLa Cx43-GFP cells expressing native Cx43 at MOI 0 or 5, based on comparisons of GJ populations ($n > 1000$ for all conditions) using a Mann–Whitney rank sum test. The difference between length distributions in HeLa Cx43-GFP and wild-type HeLa at MOI 10 was not significant.

appropriate, asterisks (*) indicate significant differences between inhibitor and no peptide treatments; hash marks (#) indicate significant differences between inhibitor and reverse peptide treatments.

RESULTS

Native Cx43 Rescues the Abnormal Cx43-GFP Gap Junction Phenotype in HeLa Cells

HeLa cells do not express significant levels of any known connexin and thus are considered communication deficient. Previously, we showed that HeLa cells stably expressing a GFP-tagged Cx43 form sheetlike GJs of abnormally large size (Hunter *et al.*, 2003); by contrast, stable expression of untagged native Cx43 resulted in small, discontinuous GJs uniformly distributed at cell–cell interfaces (Hunter *et al.*, 2003). From these observations, we concluded that fusion of GFP to the C terminus of Cx43 disrupts regulatory mechanisms that control GJ size and cellular distribution.

The fact that Cx43-GFP assembles into smaller GJs when expressed in communication-competent cells (Jordan *et al.*, 1999; our unpublished data) suggested to us that the presence of untagged native Cx43 is sufficient to rescue the abnormal GJ dynamics of Cx43-GFP. Consistent with our hypothesis, adenoviral expression of native Cx43 in HeLa Cx43-GFP cells restored GJs to normal size and organizational patterns (Figure 1). We quantified this effect by systematically modulating expression of the two Cx43 species using varying MOIs of Cx43 adenovirus and then measuring GJ lengths after 24 h of coexpression. As native Cx43 expression levels were increased in HeLa Cx43-GFP cells, the frequency of smaller GJs also increased. Complete rescue of the aberrant Cx43-GFP phenotype occurred at MOI 10 (Figure 1A), as assessed by comparison with the GJ length distributions in HeLa cells stably expressing only native Cx43 (Hunter *et al.*, 2003) or expressing only native Cx43 after adenoviral infection at MOI 10 (Figure 1A, bottom).

A shift toward smaller Cx43-GFP GJs with increased levels of native Cx43 is reflected in a plot of mean GJ lengths versus Cx43 adenovirus MOI (Figure 1B). Relative to the mean length of pure Cx43-GFP GJs, the mean length in HeLa Cx43-GFP cells coexpressing native Cx43 at MOI 10 was reduced approximately threefold and was not significantly different from the mean length in HeLa cells expressing only native Cx43 at the same MOI (Figure 1B). This convergence indicates that GJ size variation, and in particular the abnormally large size of Cx43-GFP junctions in the absence of native Cx43, is not a simple function of increasing Cx43 expression.

GJ Size Control Is Critically Dependent on Availability of Free Cx43 C Termini within the Connexon Pool

The partial reduction in mean length observed at MOI 5 (Figure 1) indicates that Cx43-GFP GJ size is normalized gradually after introduction of native Cx43 and suggests that the actual amount of native Cx43 sufficient to rescue the Cx43-GFP phenotype likely falls between that expressed by viral MOIs of 5 and 10. But exactly how much native Cx43 is

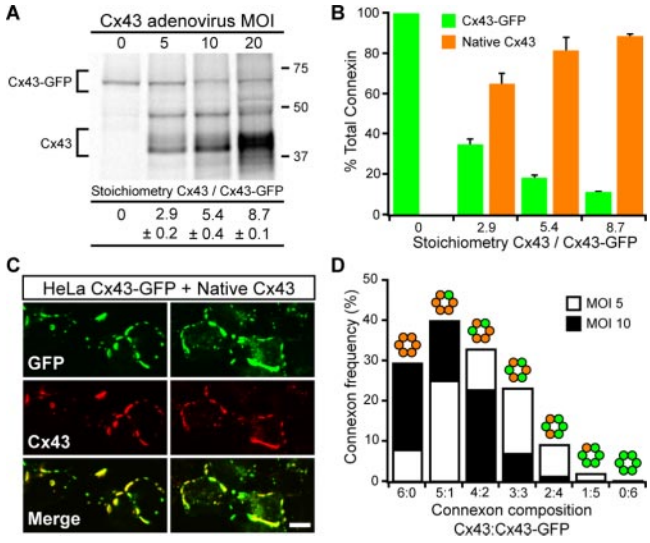

Figure 2. Reduction of Cx43-GFP plaque size by coexpression of native Cx43 requires a majority of connexons be composed predominately of native Cx43. (A) Representative gel showing changes in expression levels of Cx43-GFP and native Cx43 in HeLa Cx43-GFP cells after infection with increasing Cx43 adenovirus MOI. Connexin stoichiometries (mean ± SE; n = 3) at each MOI were determined by measuring band intensities with a PhosphorImager. (B) Connexin stoichiometries presented as bulk expression levels of Cx43-GFP and native Cx43 relative to total connexin. (C) Representative sets of confocal images showing Cx43-GFP and native Cx43 codistribute in HeLa Cx43-GFP cells coexpressing Cx43 at viral MOI 10. Note the lack of Cx43 domains devoid of GFP fluorescence. Bar, 10 μm. (D) Distribution of connexon stoichiometries expected when native Cx43 is coexpressed in HeLa Cx43-GFP at levels necessary (MOI 5) and sufficient (MOI 10) to normalize GJ size and distribution.

produced at these MOIs? More precisely, how many functional Cx43 C termini are sufficient to normalize GJ size and organizational pattern in HeLa Cx43-GFP cells?

To quantify the amounts of virally expressed native Cx43 relative to stably expressed Cx43-GFP, HeLa Cx43-GFP cells were metabolically labeled after infection with increasing amounts of Cx43 adenovirus. After immunoprecipitation, ^{35}S-labeled connexins were resolved by SDS-PAGE, and the relative amounts of the two connexin species were measured by phosphorimaging. At MOI 10—the Cx43 viral expression level sufficient for complete rescue of Cx43-GFP GJ size—we found a native Cx43:Cx43-GFP stoichiometry of ~5:1 (Figure 2A). This ratio represents a bulk distribution in rescued cells of ~80% native Cx43 versus ~20% Cx43-GFP (Figure 2B), which is consistent with a population of connexons that on average contain one or fewer Cx43-GFP molecules.

Three lines of evidence argue in favor of random mixing of native Cx43 and Cx43-GFP into heteromeric connexons. First, if tagged and untagged Cx43 segregated exclusively into homomeric connexons, then we might expect to see regions of Cx43 immunofluorescence devoid of GFP fluorescence; instead, Cx43 immunofluorescence and GFP fluorescence displayed nearly identical, overlapping patterns in cells coexpressing native Cx43 and Cx43-GFP (Figure 2C; Jordan *et al*., 1999). Second, motifs governing Cx43 oligomerization are located outside of the cytoplasmic C-terminal domain (Falk *et al*., 1997; Maza *et al*., 2005). And third, C-terminally tagged Cx43 constructs have been shown to co-oligomerize with each other and with untagged Cx43 (Lauf *et al*., 2001; Sarma *et al*., 2002). Based on knowledge of the relative expression levels of the two Cx43 species (Figure 2, A and B), and assuming random codistribution of connexins within connexons (Figure 2C), a probability equation (Burt *et al*., 2001) was used to generate the expected frequency distributions of Cx43:Cx43-GFP connexon stoichiometries (Figure 2D). The probabilistic connexon distributions suggest that when native Cx43 is expressed in HeLa Cx43-GFP cells at levels both necessary and sufficient for normalization of GJ organization (i.e., Cx43 viral expression at MOIs 5–10; Figure 1), the majority of connexons (>65%) must be composed predominately of native Cx43 (≥4 per connexon); furthermore, nearly all connexons (>99%) must contain at least one native Cx43 (Figure 2D). Clearly, a channel population comprised of connexons with a single intact Cx43 C terminus is not sufficient to reestablish GJ size control. A conservative interpretation is that connexons containing even a single Cx43-GFP cannot contribute effectively to regulation of GJ size.

C-terminal Tagging of Cx43 Does Not Interfere with Gap Junction Turnover

Connexins turn over at faster rates ($t_{1/2}$ = 1–5 h; Fallon and Goodenough, 1981; Musil *et al*., 1990; Laird *et al*., 1991; Beardslee *et al*., 1998) than most membrane proteins ($t_{1/2}$ > 24 h; Hare and Taylor, 1991). One explanation for the formation of large Cx43-GFP GJs is that they are resistant to degradation and therefore turnover more slowly than GJs composed of native Cx43. We tested this possibility using pulse-chase assays of HeLa cells expressing either native Cx43 or Cx43-GFP, or both proteins (Figure 3). Short pulse labeling (40 min) of connexin-expressing cells indicated that native Cx43 and Cx43-GFP turnover at similar rates, with half-lives ($t_{1/2}$ = 2–3 h) in the range expected for connexins (Figure 3, A and B).

Previous studies argue against the formation of a metabolically stable pool of Cx43 in GJ plaques (Laird *et al*., 1995; Musil *et al*., 2000). However, if GFP-tagged Cx43 were to segregate into pools with vastly different turnover kinetics (e.g., stable junctional versus labile nonjunctional Cx43-GFP), then short-interval metabolic labeling would not penetrate preexisting, long-lived GJs. We therefore performed long pulse labeling (≥15 h) to ensure more uniform ^{35}S-labeling in the event that the turnover rate of plaque-incorporated Cx43-GFP was appreciably slower than that of nonjunctional Cx43-GFP. However, even after protracted radiolabeling, the kinetics of Cx43-GFP turnover was not notably different from those of native Cx43 (Figure, 3, C and D). In fact, when expressed in HeLa cells, the half-life of Cx43-GFP ($t_{1/2} \approx 2$ h) seemed to be consistently shorter than that of native Cx43 ($t_{1/2} \approx$ 3–5 h; Figure 3, A–D)—a result completely at odds with the hypothesis that the abnormally large Cx43-GFP GJs arise from resistance to degradation.

When native Cx43 was coexpressed in HeLa Cx43-GFP cells, the turnover rate of both Cx43 species fell in the range of rates measured when native Cx43 was expressed alone (Figure 3E). Thus, the half-life of Cx43-GFP was *increased* slightly in the presence of native Cx43 at levels sufficient to normalize GJ size. The convergence of the half-life of Cx43-GFP to that of native Cx43 in coexpressing cells provides further evidence of random coassembly of native Cx43 and Cx43-GFP into heteromeric connexons. More importantly, the increase in Cx43-GFP half-life is opposite to what might have been expected if coexpression of native Cx43 rescued GJ size in HeLa Cx43-GFP cells by increasing the turnover rate of Cx43-GFP. These observations confirm that C-terminal tagging of Cx43 does not interfere with GJ turnover and allow us to draw an important conclusion: the abnormal size

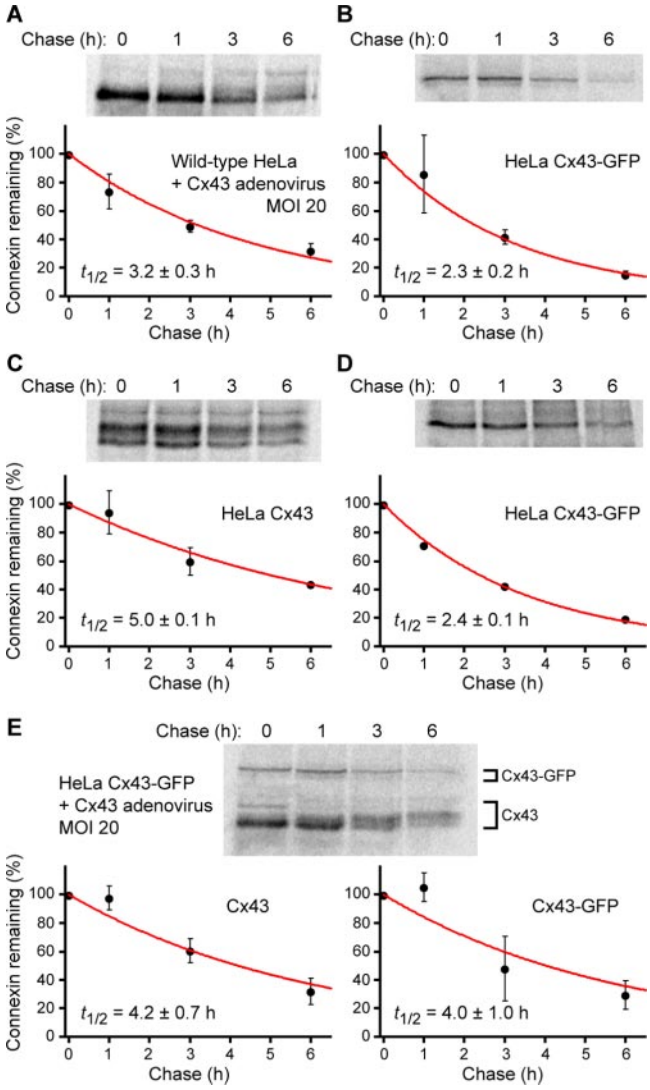

Figure 3. Native Cx43 and Cx43-GFP turnover at similar rates in HeLa cells. HeLa cells expressing native Cx43 (A and C) or Cx43-GFP (B and D) or both connexin species (E) were pulse labeled with [^{35}S]methionine for 40 min (A, B, and E) or ≥15 h (C and D), followed by chase with unlabeled methionine. At the designated times during the chase period, ^{35}S-labeled connexins were quantitatively immunoprecipitated from HeLa cells lysates and resolved using SDS-PAGE. Band intensities were measured with a PhosphorImager. Plots show levels of ^{35}S-labeled connexins remaining, normalized to the amount of ^{35}S-labeled connexin at time zero, as a function of chase time (mean ± SD; n = 2). Curves are exponential fits to the data (weighted by their uncertainties) which yielded the half-life ($t_{1/2}$) of ^{35}S-labeled connexins (mean ± SE).

of Cx43-GFP GJs cannot be explained by the formation of degradation-resistant plaques.

A Peptide Inhibitor of Cx43–ZO-1 Interaction Based on the PDZ-binding Domain of Cx43

Our results with Cx43-GFP suggested that tagging of Cx43 interfered with a regulatory mechanism that controls GJ size. C-terminal tagging of Cx43, including with GFP, has been shown by immunoprecipitation to profoundly disrupt binding of ZO-1 (Giepmans and Moolenaar, 1998; Giepmans *et al*., 2001b), suggesting a role for ZO-1 in regulating the size and organization of Cx43 GJs. However, manipulation of Cx43 through genetic tagging might affect the binding of proteins other than ZO-1. Therefore, to directly target ZO-1 activity, we synthesized a peptide comprising the PDZ-binding domain of Cx43 linked to an antennapedia internalization sequence (Figure 4A).

At concentrations between 10 and 100 μM, antennapedia peptides were detected at relatively uniform levels in cells up to 24 h after addition to culture media (Figures 4B and 5, E–F and H–I). Once inside cells, we hypothesized that the inhibitor peptide should compete for binding to ZO-1, thereby reducing its availability for interaction with the PDZ-binding domain of endogenous Cx43. As a control peptide, we used the same antennapedia sequence but reversed the Cx43 PDZ-binding sequence; thus, the reverse control peptide no longer has a free C-terminal isoleucine (Figure 4A), a Cx43 residue necessary for interaction with the second PDZ domain in ZO-1 (Giepmans and Moolenaar, 1998). In accord with our expectations, the inhibitor peptide but not the reverse peptide was pulled down by a recombinant polypeptide comprising the PDZ2 domain of ZO-1 (Figure 4C). The specificity of this interaction was corroborated by the observation that the PDZ1 domain of ZO-1 did not pull down the inhibitor or reverse peptide (Figure 4C).

Having demonstrated specificity of targeting to the PDZ2 domain, we next tested whether the inhibitor peptide disrupted ZO-1 interaction with Cx43. Inhibitor or control peptides were added to lysates from HeLa Cx43 cells and then either the PDZ1 or PDZ2 domains of ZO-1 were used to pull down Cx43. Consistent with interference of Cx43–ZO-1 binding, the amount of Cx43 pulled down by PDZ2 in the presence of inhibitor peptide was significantly reduced relative to Cx43 pulled down in the presence of control peptide or no peptide (Figure 4D). As expected, no Cx43 was pulled down by PDZ1 irrespective of the presence or absence of peptides. Based on these data, we conclude that the inhibitor peptide disrupts the interaction between Cx43 and ZO-1.

Disruption of Cx43–ZO-1 Interaction Increases the Size of Cx43 GJs

To characterize the effects of the inhibitor peptide on GJs, HeLa Cx43 cells were treated with the inhibitor, reverse, or no peptide for 72 h. At the end of the culture period, living cells were first exposed to TRITC-WGA to label cell membranes and then fixed and immunolabeled for Cx43 (Figure 5, A–F). As shown qualitatively in Figure 5, A–C, exposure to the inhibitor peptide resulted in increased levels of Cx43 at WGA-defined cell membranes relative to controls. Increased cell border-localized Cx43 also was observed in primary cultures of neonatal cardiomyocytes treated with inhibitor peptide (Figure 5I).

Quantitatively, treatment with inhibitor peptide increased the average dimensions of individual Cx43 plaques in both HeLa Cx43 cells and neonatal cardiomyocytes relative to controls (Figure 6A). This increase in mean GJ size in response to inhibitor peptide was highly significant with larger GJs occurring at greater frequency (at the expense of smaller GJs) in both cell types (Figure 6B). In addition to increased GJ size, the total area of membrane-localized plaques in HeLa Cx43 cells was significantly increased by exposure to inhibitor peptide relative to no peptide controls (Figure 6C); and consistent with increased plaque fusion (or decreased fission) events, HeLa Cx43 cells showed a slight reduction in the number of membrane-localized GJs in inhibitor-treated versus control cells (Figure 6D), although we could not establish this as a definitive trend.

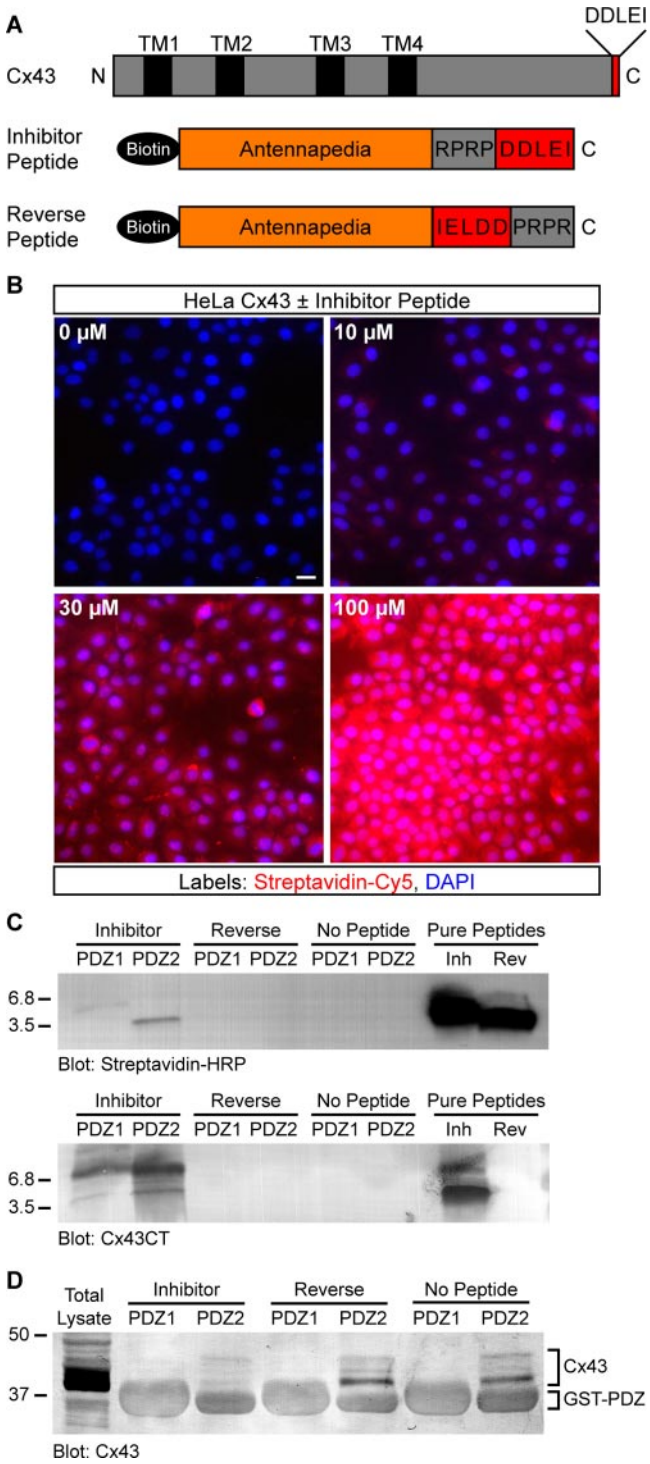

Figure 4. A peptide inhibitor that binds specifically to the second PDZ domain of ZO-1 and blocks interaction with Cx43. (A) Domain organization of full-length Cx43 and antennapedia peptides. (B) Detection of biotinylated peptide (0–100 μM) in HeLa cells after 2 h. Streptavidin-Cy5 fluorescence intensity shows a dose-dependent increase with increasing peptide concentration. Cell nuclei are stained with DAPI. Bar, 15 μm. (C) Western blots showing that inhibitor and reverse peptides (~3.5 kDa) both were detected by streptavidin-HRP (top blot), but only inhibitor peptide was detected by an antibody that recognizes the C terminus of Cx43 (bottom blot). Only inhibitor peptide was pulled down by purified ZO-1 GST-PDZ2 fusion protein-coupled beads; neither peptide was pulled down by GST-PDZ1 beads. (D) Representative Cx43 blot showing that the amount of endogenous Cx43 pulled down from HeLa lysates by GST-PDZ2 beads was significantly reduced by the presence of inhibitor peptide. Peptide inhibition of PDZ2-Cx43 interaction was reproducible (n = 3). Comparison of nonspecific GST fusion protein band intensities confirms equal loading across conditions.

We can rule out the possibility that the observed increases in plaque size (Figure 6A) and overall levels of immunodetectable Cx43 GJs at cell–cell borders (Figure 6C) were due simply to an increase in Cx43 expression, because the inhibitor peptide did not significantly affect the total amount of Cx43 in HeLa cells or cardiomyocytes (Figure 6E). This agrees with the recent observation that Cx43 abundance was unaltered after disruption of Cx43–ZO-1 interaction in osteoblastic cells (Laing *et al.*, 2005). Moreover, this accords with our finding that the size of Cx43-GFP plaques was reduced after *increasing* the expression of native Cx43 (Figures 1 and 2).

Collectively, the data presented in Figure 6 suggest that the observed increase in GJ plaque size in the presence of the inhibitor peptide is due mainly to unregulated accretion of connexons from nonjunctional pools, with a possible contribution from increased plaque fusions.

Peptide Inhibition of Cx43–ZO-1 Interaction Leads to Redistribution of Cx43 from Nonjunctional Pools to GJ Plaques

Unaltered levels of total Cx43 in peptide-treated cells (Figure 6E) suggested that, rather than accumulation of newly upregulated Cx43, the increased dimensions of individual Cx43 plaques at cell borders might be due to a redistribution of preexisting Cx43. We tested this possibility using a biochemical fractionation assay that distinguishes junctional from nonjunctional connexins. HeLa Cx43 cells were treated with peptides for 72 h and then lysed in ice-cold buffer containing 1% Triton X-100. Under these conditions nonjunctional connexins are solubilized, whereas GJ plaques remain insoluble (Musil and Goodenough, 1991). After lysis, the two populations of connexins were fractionated by centrifugation and resolved using SDS-PAGE. The Triton-soluble fraction resolves predominately as an indistinguishable collection of faster-migrating isoforms (NP/P0) that represent nonjunctional Cx43, which is largely (although not exclusively) unphosphorylated (Figure 7A; Musil and Goodenough, 1991; Solan *et al.*, 2003). In contrast, the Triton-insoluble gap junctional fraction resolves as at least three distinct Cx43 isoforms, NP/P0 and two phosphorylated species, P1 and P2 (Figure 7A).

Generally, it is thought that unphosphorylated Cx43 assembles into connexons en route to the plasma membrane (Musil and Goodenough, 1991; Musil and Goodenough, 1993). Phosphorylation events that result in gel mobility shifts occur subsequent to delivery to the plasma membrane and are closely linked to accretion of connexons into Triton-insoluble GJ plaques (Musil and Goodenough, 1991). The banding patterns shown in Figure 7A follow the well-established relationship between detergent solubility, gel mobility, and phosphorylation state with respect to the life cycle of connexins (Musil and Goodenough, 1991). Band intensity profiles reveal a shift in the relative amounts of the various Cx43 isoforms after treatment with inhibitor peptide (Figure 7B). Quantitative densitometry showed that the inhibitor peptide caused a significant reduction in the level of soluble relative to insoluble Cx43 (Figure 7C), which suggests

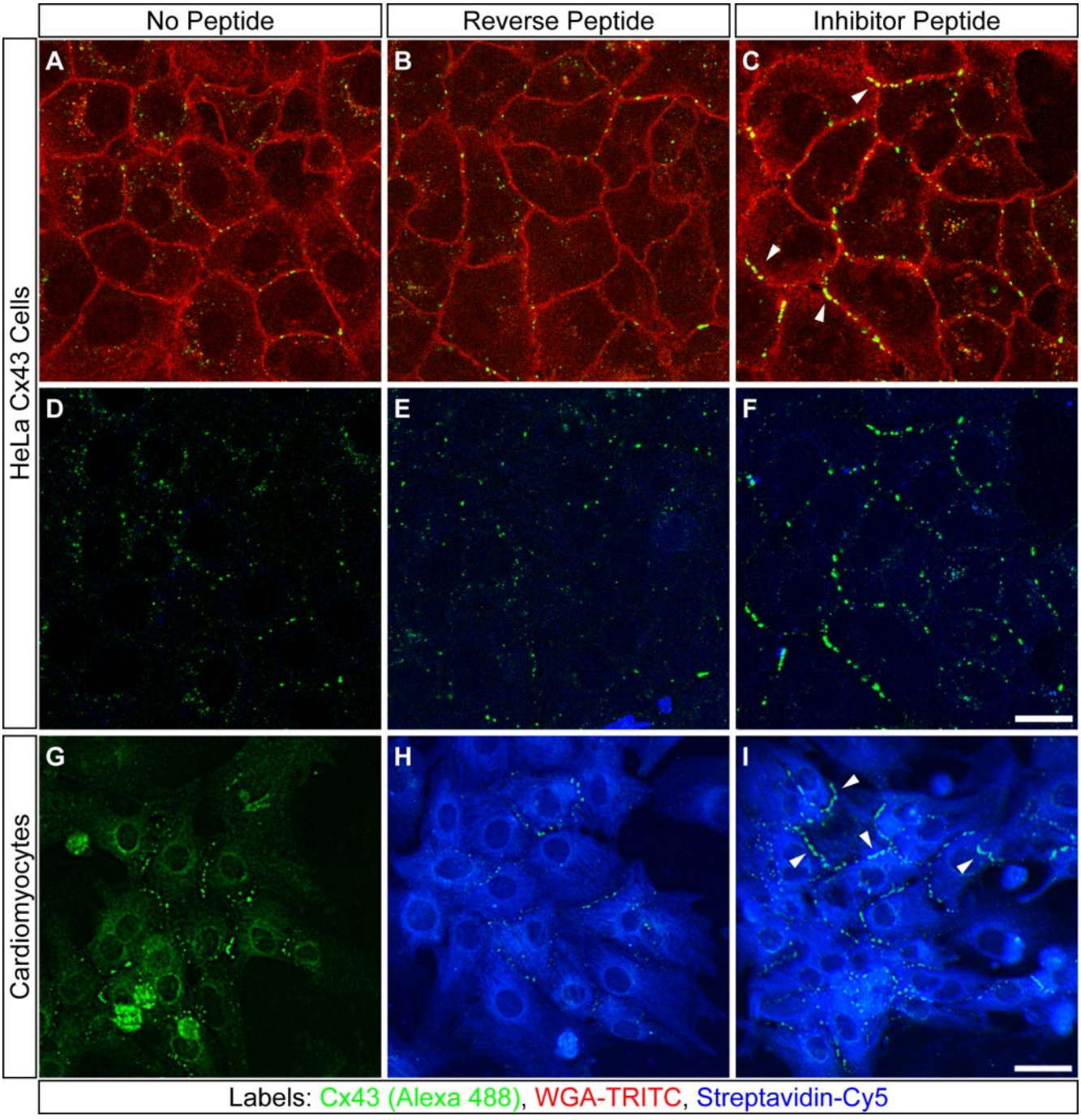

Figure 5. Peptide inhibition of Cx43–ZO-1 interaction increases the extent of membrane-localized Cx43 GJ plaques in HeLa cells and cardiomyocytes. Confocal optical sections of HeLa Cx43 cells (A–F) and neonatal cardiomyocytes (G–I) cultured for 72 or 24 h, respectively, without peptide (A, D, and G), or with reverse (B, E, and H) or inhibitor peptide (C, F, and I). All cells were immunolabeled for Cx43 (A–I). Peptides were detected with streptavidin-Cy5 (D–I). WGA-TRITC delineates HeLa cell membranes (A–C). Arrowheads (C and I) denote accumulation of membrane-localized Cx43 plaques in inhibitor-treated cells. Bars, 20 μm (A–F); 80 μm (G–I).

greater incorporation of connexons into GJ plaques. Furthermore, within the insoluble fraction, we detected a significant increase in the amounts of the P1 and P2 phosphoisoforms relative to controls (Figure 7D). The increases in Cx43-P1 and -P2 seemed to be linked because the ratio of P2/P1 was not affected by peptide treatment (Figure 7D). The increase in Triton-insoluble Cx43, in conjunction with the appearance of elevated levels of phosphorylated Cx43 species known to populate mature GJs, supports the idea that the inhibitor peptide increases GJ size by promoting the accretion of nonjunctional connexons into gap junctional plaques.

ZO-1 Localization at GJ Peripheries Depends on PDZ-mediated Interaction with Cx43

In addition to increasing the extent of Cx43 GJs, both C-terminal tagging of Cx43 and the inhibitor peptide had

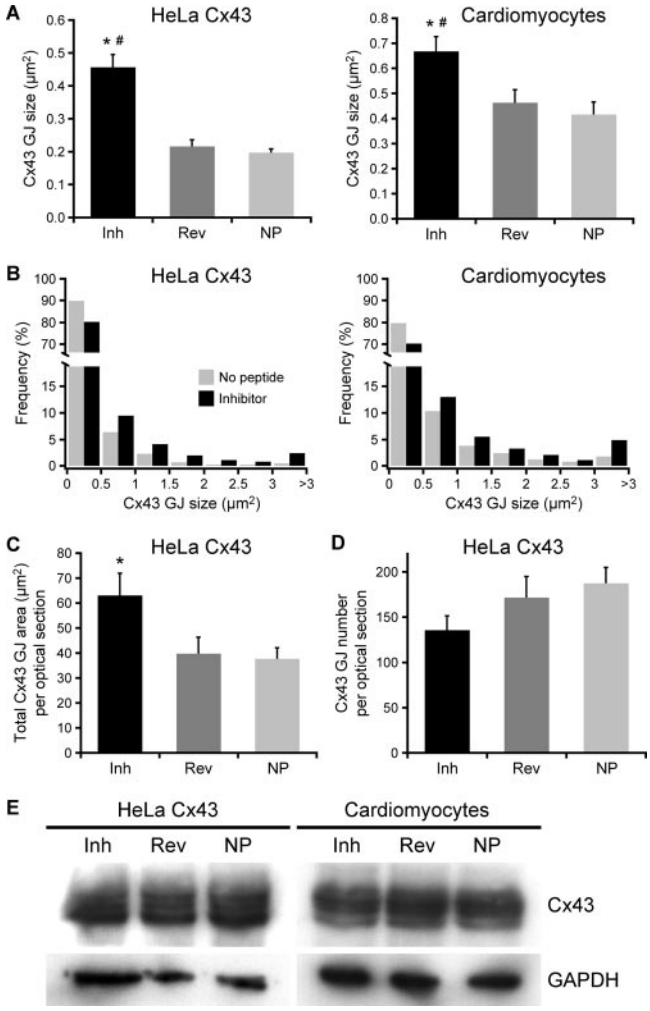

Figure 6. Quantification of gap junction patterning in HeLa cells and cardiomyocytes after peptide inhibition of Cx43–ZO-1 interaction. (A) The area of individual Cx43 plaques increased significantly (*#$p \leq 0.001$) after 72 h (HeLa Cx43) and 48 h (cardiomyocytes) treatments with inhibitor peptide relative to controls (means ± SE; $n \geq 30$). (B) Size distributions of Cx43 plaques in cells treated with inhibitor or no peptide. Inhibitor distributions are significantly different (chi-square test yielded *#$p < 0.001$; $n \geq 780$ for all conditions) from control distributions (reverse peptide distributions omitted for clarity). (C) Total area of membrane-localized Cx43 plaques was increased significantly (*$p = 0.013$) by inhibitor peptide (means ± SE; $n \geq 30$). (D) Cells treated with inhibitor peptide displayed a slight reduction in GJ number (means ± SE; $n \geq 30$). (E) Western blots of HeLa and cardiomyocyte lysates show that peptide treatment does not alter Cx43 protein expression levels. GAPDH blots serve as loading controls.

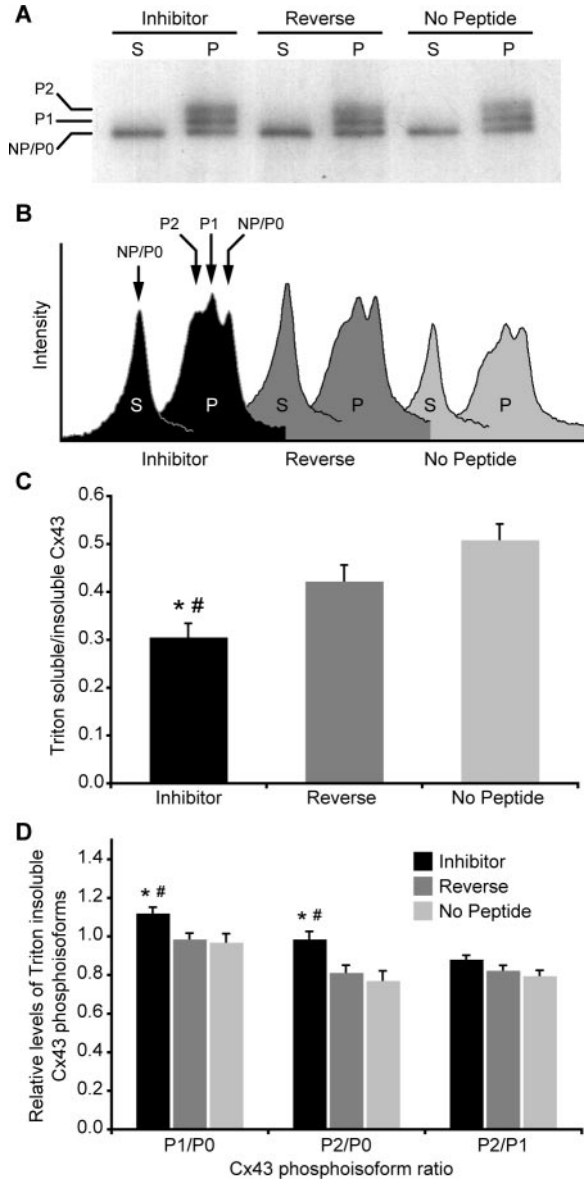

Figure 7. The formation of larger GJ plaques after disruption of Cx43–ZO-1 interaction results from a redistribution of Cx43. (A) Representative gel of Triton fractionation assay. (B) Corresponding plot of band intensities generated by densitometric analysis. Note the change in peak profiles in the inhibitor condition. (C) Shifts in subcellular Cx43 distribution are expressed as ratios of fractionated Cx43 isoforms. Exposure to inhibitor peptide for 72 h significantly reduced (*$p = 0.0001$; #$p = 0.015$) the level of Triton-soluble relative to Triton-insoluble Cx43 in HeLa cells. (D) The shift of Cx43 from soluble to insoluble pools induced by inhibitor peptide was accompanied by significant increases in Cx43-P1 (*$p = 0.012$; #$p < 0.006$) and -P2 (*$p \leq 0.003$; #$p < 0.005$) phosphoisoforms (relative to NP/P0) within the insoluble fraction.

effects on the pattern of colocalization between ZO-1 and Cx43 (Figure 8). Interestingly, ZO-1 was often seen associated at the peripheries of GJs in HeLa Cx43 cells (Figure 8A). By contrast, ZO-1 localization in HeLa Cx43-GFP cells seemed to be independent of GJs (Figure 8B). Although ZO-1 staining was seen along the edges of some large Cx43-GFP plaques (Figure 8B, insets), this localization seemed to be coincidental, with no evidence of actual overlap. However, when native Cx43 was coexpressed in HeLa Cx43-GFP cells, colocalization of ZO-1 at plaque peripheries was reestablished (Figure 8C, insets). This suggests that the mechanistic link between restoration of ZO-1 localization at GJ peripheries and size reduction of aberrantly large Cx43-GFP GJs is the formation—after introduction of native Cx43—of heteromeric connexons that are competent to bind ZO-1.

Similar to the HeLa Cx43-GFP phenotype, isolated cardiomyocytes treated with the inhibitor peptide produced larger GJs that seemed to have less colocalized ZO-1 than GJs in control cells (Figure 8, D–F). Again, most of the ZO-1 that colocalized with Cx43 in cardiomyocytes seemed re-

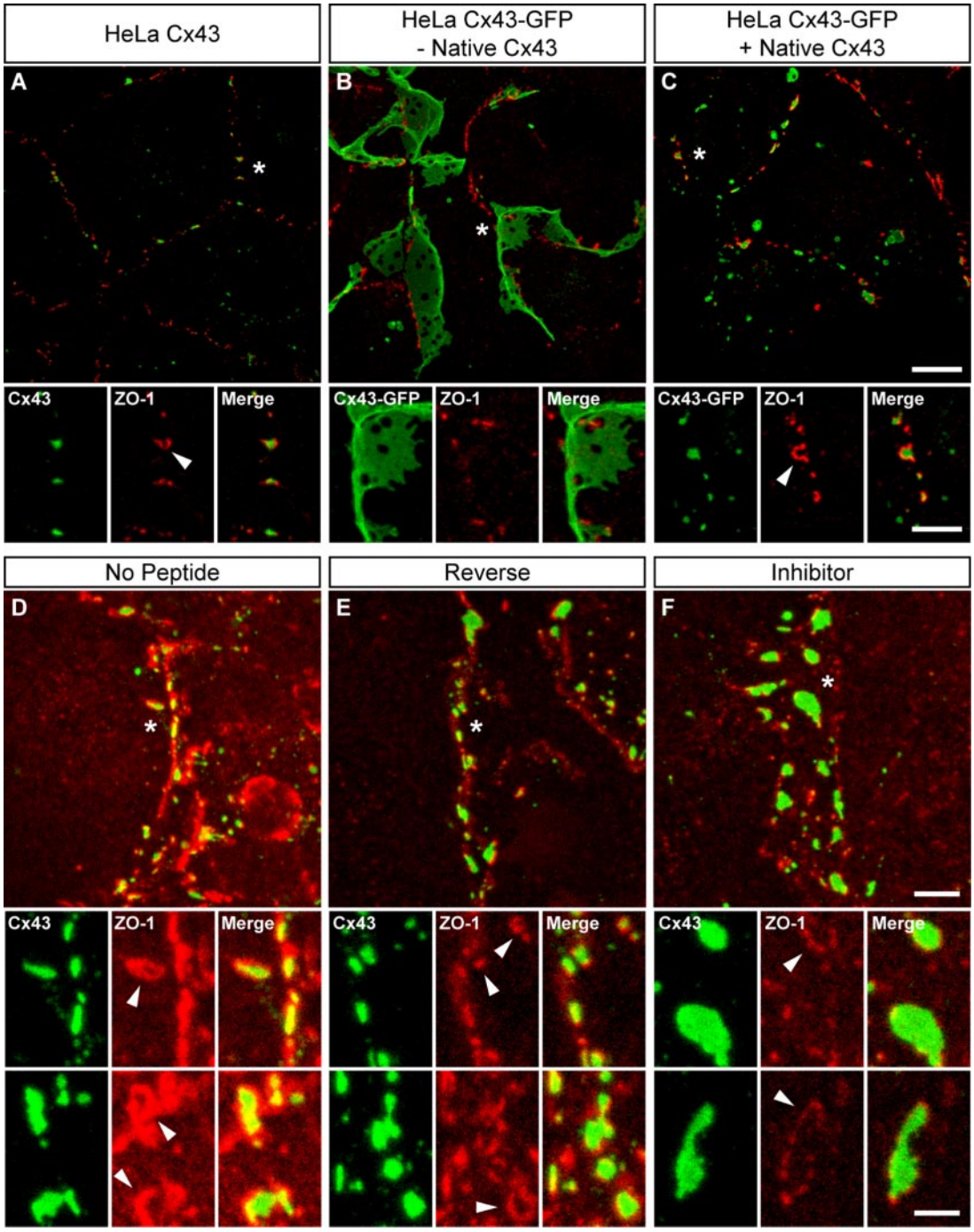

Figure 8. Disruption of Cx43–ZO-1 interaction reduces the preferential association of ZO-1 with the perimeter of Cx43 GJ plaques. (A–C) Maximum projection *z*-series of HeLa cells expressing native Cx43 (A), Cx43-GFP (B), or both GFP-tagged and native Cx43 (C). After 24 h, cells were fixed and immunolabeled for Cx43 and ZO-1. Note that ZO-1 localizes to the periphery of small, discontinuous native Cx43 GJ plaques (A, arrowhead) but is excluded from large, sheetlike Cx43-GFP plaques (B). Coexpression of native Cx43 (viral MOI 5) in HeLa Cx43-GFP cells reduces plaque size and restores ZO-1 colocalization at plaques perimeters (C, arrowhead). (D–F) Maximum projection *z*-series of neonatal cardiomyocytes treated for 48 h with the inhibitor (F), reverse (E), or no peptide (D). Note the striking pattern of ZO-1 colocalization with Cx43 plaque edges (D–F, arrowheads), which is reduced in inhibitor-treated cells. Asterisks (*) in top panels (A–F) denote image areas enlarged in lower panels (the second set of bottom panels in D–F are enlargements from different images). Bars, 10 μm (A–C, top); 5 μm (A–C, bottom); 5 μm (D–F, top); 2.5 μm (D–F, bottom).

stricted to the periphery of GJ plaques rather than their interior. In fact, some plaques displayed near continuous runs of ZO-1 that circumscribed the perimeter of the GJ; however, only a fraction of ZO-1 at plaque perimeters seemed to overlap directly with Cx43 (Figure 8, D–F, arrowheads).

Quantitative analysis of confocal images confirmed that the inhibitor peptide reduced ZO-1 colocalization with Cx43

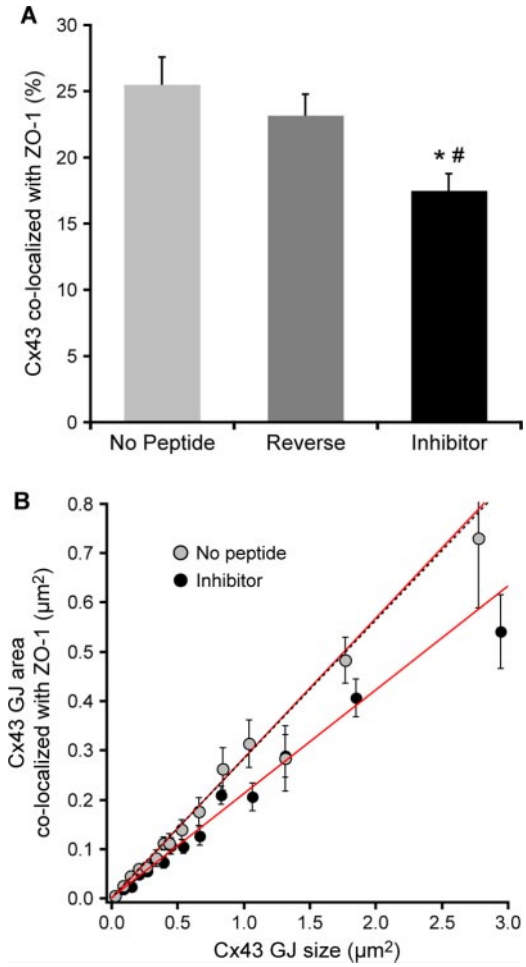

Figure 9. Quantitative image analysis of ZO-1 association with Cx43 GJs after peptide inhibition. (A) The average level of ZO-1 colocalization within individual plaques Cx43 (means ± SE) was significantly reduced (*$p = 0.001$; #$p = 0.006$) in inhibitor-treated cardiomyocytes. (B) Cx43 area colocalized with ZO-1 (means ± SE) as a function of GJ size in myocytes. GJ sizes are means derived from binned data. Lines are linear regression fits weighted by uncertainties in GJ area colocalized with ZO-1; black dotted line is the fit to the reverse peptide data (omitted for clarity). Slopes correspond to the fractional area of individual Cx43 plaques colocalized with ZO-1, which was significantly reduced (*#$p < 0.001$) in inhibitor-treated cells.

GJs. The average area of individual Cx43 plaques colocalized with ZO-1 was decreased significantly in isolated cardiomyocytes treated for 48 h with the inhibitor (17.5 ± 1.3%) compared with reverse (23.1 ± 1.6%) and no peptide (25.5 ± 2.0%) controls (Figure 9A). Fitting a line to a plot of the area of Cx43 colocalized with ZO-1 versus GJ size (Figure 9B) revealed a positive correlation ($r \geq 0.7$ for each condition when data were weighted by their uncertainties) between GJ size and the area of colocalized ZO-1 that was independent of peptide treatment. However, the differential effects of the peptide treatments were manifest as a significant decrease in the slope (equal to ZO-1 colocalization as a percentage GJ area) of the line fitted to the inhibitor data (21.08 ± 0.008%) relative to the slopes derived from fits to the reverse (28.23 ± 0.009%) and no peptide (28.43 ± 0.011%) control data (Figure 9B). Plaques >3.44 μm^2 were excluded from the fitting process due to a single nonlinear outlier in the no peptide data at these GJ sizes. Nevertheless, the colocalization values associated with GJs >3.44 μm^2 in cells treated with either the inhibitor or reverse peptide fell within the 95% confidence interval for the linear fits shown in Figure 9B. Because the data were weighted by their uncertainties for linear regression analysis (Figure 9B), mean colocalization values obtained from linear fits differ slightly from those calculated by unweighted averaging (Figure 9A).

Linear extrapolation of the data for the different peptide conditions did not produce significantly different intercepts; interestingly, however, the intercepts for all three conditions were significantly different from zero (Inh $p < 0.002$, Rev $p < 0.005$, and NP $p < 0.001$) and were consistently negative values, which correspond to positive ordinal intercepts (Figure 9B). This suggests that, rather than being coassembled with Cx43, ZO-1 is recruited to GJs after they reach a critical size. Taking the average of the ordinal intercepts (assuming that the intercepts from the three conditions are equivalent) yielded a critical GJ size of 9300 ± 400 $nm^2 \approx 100$ channels, assuming 90-Å center-to-center hexagonal packing.

Together, the similar disruptive effects of the inhibitor peptide and C-terminal tagging of Cx43 show that localization of ZO-1 to GJ plaques is likely dependent on a binding interaction between the C terminus of Cx43 and the PDZ2 domain of ZO-1.

DISCUSSION

The shape, extent, and distribution of gap junctional plaques are recognized as important variables in the regulation of intercellular coupling (Evans and Martin, 2002) and coupling-dependent processes such as action potential spread in heart and brain (Severs *et al*., 2004). Here, we provide evidence that reduction in ZO-1 interaction with Cx43 is associated with increases in the size of GJ plaques. First, we demonstrated that disruption of ZO-1 binding by genetic tagging of the C terminus of Cx43 with GFP leads to the formation of abnormally large GJs when the tagged construct is expressed in connexin-deficient HeLa cells; the abnormal Cx43-GFP phenotype was rescued by coexpression of significant levels of native Cx43 (>80% of the total connexin). Second, we showed that targeted disruption of Cx43–ZO-1 interaction using a peptide inhibitor based on the PDZ-binding domain of Cx43 also caused a significant increase in the mean size of Cx43 GJs in two cell types, primary neonatal cardiomyocytes and a HeLa cell line expressing native Cx43. Third, we found that the increase in GJ size arose from a redistribution of Cx43 from nonjunctional pools to GJ plaques, with a possible contribution from increased plaque fusion events. And finally, both GFP tagging and the inhibitor peptide caused a significant reduction in the amount of ZO-1 associated at the peripheries of GJ plaques. Together, these data suggest a function for ZO-1 in regulating the growth of Cx43 GJs by controlling the rate at which connexons are incorporated into GJ plaques at their peripheries.

Previously, we demonstrated that ZO-1 shows low-to-moderate levels of colocalization with Cx43 GJs in adult rat heart (Barker *et al*., 2002). The present study confirms and extends this finding, demonstrating quantitatively in isolated cardiomyocytes that colocalization between ZO-1 and Cx43 in individual GJ plaques is limited to ~28% overlap (Figure 9B). Likewise, Nielsen *et al*. (2003) found that the overall extent of colocalization between ZO-1 and Cx46 or Cx50 in the eye lens was limited. Duffy *et al*. (2004) have also confirmed in cultured astrocytes that colocalization of ZO-1 with Cx43 at cell borders is confined to a partial overlap.

Overall, the data suggest that in astrocytes, lens and heart a significant proportion of the connexin pool localized at cell borders does not associate with ZO-1.

What then is the functional significance of the limited interaction between ZO-1 and connexins? The high resolution confocal images presented here provide a detailed perspective of the spatial relationship between ZO-1 and Cx43 within GJ plaques. These images reveal that the majority of ZO-1 does not overlap directly with plaque interiors; rather, ZO-1 seems to associate preferentially with the edges of GJs. EM data from Li *et al*. (2004) also support the idea that ZO-1 associates preferentially with the perimeter of GJ plaques. That the perimeter is a specialized microdomain of GJ plaques was established by studies that demonstrated that addition of C-terminal-tagged Cx43 occurred at the periphery of GJ plaques (Gaietta *et al*., 2002; Lauf *et al*., 2002). Although there seems to be a general spatial correlation between ZO-1 and sites of connexin recruitment into GJs, it is unlikely that ZO-1 enhances GJ assembly because C-terminal-truncated forms of Cx43 lacking the ZO-1 binding domain are able to form functional GJs (Fishman *et al*., 1991; Liu *et al*., 1993). More specifically, mutations targeting the PDZ-binding domain of Cx43 and other connexins known to interact with ZO-1 suggest that ZO-1 is dispensable for the formation or ongoing aggregation of connexons into functional GJs (Toyofuku *et al*., 2001; Nielsen *et al*., 2003; Li *et al*., 2004). Likewise, fusion of epitope tags or GFP to the C terminus of Cx43, which results in loss of ZO-1 binding (Giepmans and Moolenaar, 1998; Giepmans *et al*., 2001b), does not impede the formation of GJ plaques (Jordan *et al*., 1999; Bukauskas *et al*., 2000; Gaietta *et al*., 2002; Lauf *et al*., 2002; Hunter *et al*., 2003). Furthermore, as we show here, reduction of Cx43–ZO-1 interaction increases rather than decreases the size of Cx43 plaques. Collectively, these data indicate that a role for ZO-1 in promoting the formation and growth of GJ plaques, although not ruled out, is unlikely.

Based on increased Cx43–ZO-1 colocalization after enzymatically or chemically induced GJ internalization, we and others have postulated that reduction of ZO-1 binding to Cx43 inhibits GJ internalization via formation of so-called annular GJs. (Barker *et al*., 2002; Segretain *et al*., 2004). However, our analysis of Cx43-GFP turnover in HeLa cells argues strongly against an explanation for the redistribution of Cx43 and plaque expansion resulting from peptide inhibition of Cx43–ZO-1 interaction based solely on suppression of GJ internalization. Cx43-GFP, a connexin incompetent to interact with ZO-1, was found to turnover at a rate nearly identical to that of native Cx43 (Figure 3). Thus, GJs comprised exclusively of Cx43-GFP, despite being abnormally large, continue to turnover with a half-life ($t_{1/2} \approx 2$ h) consistent with turnover rates in vivo (Fallon and Goodenough, 1981; Beardslee *et al*., 1998) and with other systems expressing tagged Cx43 (Gaietta *et al*., 2002; Segretain and Falk, 2004). Moreover, cells expressing Cx43-GFP generate annular GJs (Laird *et al*., 2001; Segretain and Falk, 2004), a finding we have confirmed using live imaging of HeLa Cx43-GFP cells (our unpublished data). And although Duffy *et al*. (2004) confirmed coassociation between Cx43 and ZO-1 during enzymatically induced Cx43 internalization in astrocytes, pH-induced internalization of Cx43 was preceded by a *loss* of Cx43–ZO-1 interaction. Therefore, increased Cx43–ZO-1 colocalization after certain membrane internalization events remains an unresolved issue, but it seems to be independent of normal Cx43 turnover. Finally, if ZO-1 were to play a prominent role in GJ internalization we might expect to see ZO-1 localize preferentially to the center of GJs—the major site of plaque removal—rather than the GJ periphery—the major site of plaque assembly. Together, these findings provide strong evidence against the direct involvement of ZO-1 in the machinery of GJ internalization and/or degradation.

Disruption of Cx43–ZO-1 interaction does seem to be associated with unconstrained growth of Cx43 channel aggregates. We propose that ZO-1 actively constrains GJ size by regulating the rate of channel accretion. Qualitatively, the preferential localization at the perimeter of GJ plaques places ZO-1 in a prime location—the site of plaque assembly—to play a role in control of connexon incorporation into GJs. But the most compelling evidence for ZO-1 control of connexon accretion comes from observations that the inhibitor peptide caused a quantitative reduction in the amount of ZO-1 colocalized within individual plaques, concomitant with quantitative increases in Triton-insoluble Cx43 (at the expense of the Triton-soluble pool) and plaque size. We think these events are linked causally, which makes sense. Even a slight reduction in ZO-1 binding at plaque perimeters might allow connexon accretion to proceed at a faster rate. If the turnover rate remained constant, then an increase in the rate of channel aggregation would be expected over time to result in larger GJ plaques. Likewise, if the rate of connexon accretion increased but connexin expression remained constant, then we would expect to see an increase in junctional (i.e., Triton-insoluble) Cx43 relative to nonjunctional (i.e., Triton-soluble) Cx43. Our combined data sets fit both the conditions and the expectations of the above-mentioned suppositions. The appearance of increased levels of Triton-insoluble Cx43-P1 and -P2 isoforms, both of which are constituents of mature GJs (Musil and Goodenough, 1991), in inhibitor-treated cells lends further support to our proposal that ZO-1 plays a role in connexon accretion.

Importantly, although we think ZO-1 controls the rate of connexon accretion and therefore exerts a level of control over plaque expansion, ZO-1 does not sense GJ size. We infer this from the linear relationship between GJ size and the level of ZO-1 associated with individual plaques: ZO-1 continues to associate with larger GJs at levels equivalent (in terms of percentage of plaque coverage) to that of smaller GJs (Figure 8H). This suggests that subsequent to plaque nucleation the mechanism of ZO-1 recruitment to GJs operates irrespective of plaque size. Thus, ZO-1 does not seem to cap GJ size in absolute terms. Instead, the average GJ size at steady state is set by a combination of the rates of connexon accretion and GJ turnover.

Our conclusion that ZO-1 constrains the growth of GJs is seemingly at odds with the findings of Laing *et al*. (2005), who reported reduced appositional Cx43 immunostaining and decreased GJ-mediated dye transfer after overexpression of a dominant-negative ZO-1 mutant in osteoblastic cells. It is noteworthy that the truncated mutant used by Laing *et al*. (2005) included N-terminal regions of ZO-1 that extend beyond the PDZ2 domain, including the entire PDZ1 domain. The N-terminal half of ZO-1 is known to be a functional component in cadherin-based cell adhesion (Itoh *et al*., 1997). In fact, a truncated ZO-1 mutant similar to that of Laing *et al*. (2005) was shown to disrupt cadherin-based adherens junctions (AJs; Ryeom *et al*., 2000). Because AJs are prerequisite for the formation and maintenance of Cx43 GJs (Meyer *et al*., 1992; Hertig *et al*., 1996; Wei *et al*., 2005), the effects of the Laing *et al*. (2005) mutant could be interpreted as secondary due to decreased GJ stability, rather than caused directly by loss of ZO-1 binding to Cx43.

Left unanswered is the question of how ZO-1 arrives at plaque perimeters. Much of the ZO-1 that surrounds GJs does not colocalize with Cx43. Presumably, ZO-1 not asso-

ciated directly with Cx43 at plaque edges is complexed with another cell junction type, the obvious candidate being the AJ. The recent discovery that Cx43 coassembles with N-cadherin (Wei *et al*., 2005) raises the possibility that AJs nucleate GJs, with ZO-1 recruited first to AJs then passed along to Cx43 once the GJ achieves a critical density of channels, as suggested by our colocalization analysis (Figure 9B). Thus, it is unsurprising that overexpression of ZO-1 can lead to enhanced GJ-mediated dye transfer (Laing *et al*., 2005) because ZO-1 might promote the formation of AJs, which in turn serve as GJ nucleation sites. The important point is that ZO-1 does not inhibit the formation of GJs, we think it merely constrains the rate of GJ growth after they form.

The recent finding that ZO-2 also binds to the C terminus of Cx43 (Singh *et al*., 2005) presents the intriguing prospect that ZO-1 and ZO-2 compete for influence over Cx43 GJ patterning. Because both ZO proteins interact with the PDZ-binding motif in Cx43, the effects of our genetic tagging and peptide inhibition on GJ size control might be influenced by alterations in the activity of ZO-2 as well as ZO-1. At present, we cannot exclude this possibility, but given that Cx43 interacts predominately with ZO-1 in quiescent cells (Singh *et al*., 2005), the effects of peptide inhibition in post-mitotic cardiomyocytes reported here are likely due to the specific disruption of ZO-1 activity. Nevertheless, distinguishing the activities of ZO-1 and ZO-2 with respect to Cx43 GJ dynamics poses a formidable challenge, especially considering the potential for functional redundancy and compensation (Umeda *et al*., 2004).

Finally, control of Cx43 channel accretion has important consequences for the regulation of GJ-mediated cell–cell communication versus cell communication with the extracellular environment via hemichannels (Goodenough and Paul, 2003). Channel clustering is thought to lead to activation of individual intercellular channels within GJ plaques (Bukauskas *et al*., 2000). A natural assumption is that by controlling the rate of channel aggregation, ZO-1 directly influences the level of cell–cell communication. But by limiting connexon incorporation into GJ plaques, ZO-1 might also effectively maintain a pool of nonjunctional Cx43 hemichannels that remain free to communicate with the extracellular space. Changes in the rate of connexon accretion by modulating ZO-1 action at plaque perimeters might then be expected to provide a control point for dynamic switching between junctional and nonjunctional communication mediated by Cx43 channels. In conjunction with fast turnover rates, this type of control offers the possibility of shifting the balance from one type of communication to the other on relatively rapid time scales, thus allowing cells to respond quickly to changes in their environment.

ACKNOWLEDGMENTS

We thank Dr. Ben Giepmans for ZO-1 GST-PDZ fusion proteins, assistance with turnover assays, and helpful discussion; Jane Jourdan and Dr. Yuhua Zhang for technical assistance; Dr. Stewart Denslow for advice on statistics; Dr. Klaus Willecke for HeLa Cx43 cells; and Dr. Dale Laird for the Cx43-GFP construct. This work was supported by National Institutes of Health Grants HL07260 (to A.W.H.) and HL56728, HL36059, and HD39946 (to R.G.G.).

REFERENCES

Anderson, J. M. (1996). Cell signalling: MAGUK magic. Curr. Biol. *6*, 382–384.

Barker, R. J., Price, R. L., and Gourdie, R. G. (2002). Increased association of ZO-1 with connexin43 during remodeling of cardiac gap junctions. Circ. Res. *90*, 317–324.

Beardslee, M. A., Laing, J. G., Beyer, E. C., and Saffitz, J. E. (1998). Rapid turnover of connexin43 in the adult rat heart. Circ. Res. *83*, 629–635.

Bukauskas, F. F., Jordan, K., Bukauskiene, A., Bennett, M. V., Lampe, P. D., Laird, D. W., and Verselis, V. K. (2000). Clustering of connexin 43-enhanced green fluorescent protein gap junction channels and functional coupling in living cells. Proc. Natl. Acad. Sci. USA *97*, 2556–2561.

Burt, J. M., Fletcher, A. M., Steele, T. D., Wu, Y., Cottrell, G. T., and Kurjiaka, D. T. (2001). Alteration of Cx *43*, Cx40 expression ratio in A7r5 cells. Am. J. Physiol. *280*, C500–C508.

Defamie, N., Mograbi, B., Roger, C., Cronier, L., Malassine, A., Brucker-Davis, F., Fenichel, P., Segretain, D., and Pointis, G. (2001). Disruption of gap junctional intercellular communication by lindane is associated with aberrant localization of connexin43 and zonula occludens-1 in 42GPA9 Sertoli cells. Carcinogenesis *22*, 1537–1542.

Duffy, H. S., Ashton, A. W., O'Donnell, P., Coombs, W., Taffet, S. M., Delmar, M., and Spray, D. C. (2004). Regulation of connexin43 protein complexes by intracellular acidification. Circ. Res. *94*, 215–222.

Dupont, E., Matsushita, T., Kaba, R. A., Vozzi, C., Coppen, S. R., Khan, N., Kaprielian, R., Yacoub, M. H., and Severs, N. J. (2001). Altered connexin expression in human congestive heart failure. J. Mol. Cell Cardiol. *33*, 359–371.

Evans, W. H., and Martin, P. E. (2002). Gap junctions: structure and function (Review). Mol. Membr. Biol. *19*, 121–136.

Falk, M. M., Buehler, L. K., Kumar, N. M., and Gilula, N. B. (1997). Cell-free synthesis and assembly of connexins into functional gap junction membrane channels. EMBO J. *16*, 2703–2716.

Fallon, R. F., and Goodenough, D. A. (1981). Five-hour half-life of mouse liver gap-junction protein. J. Cell Biol. *90*, 521–526.

Fishman, G. I., Hertzberg, E. L., Spray, D. C., and Leinwand, L. A. (1991). Expression of connexin43 in the developing rat heart. Circ. Res. *68*, 782–787.

Fonseca, C. G., Green, C. R., and Nicholson, L. F. (2002). Upregulation in astrocytic connexin 43 gap junction levels may exacerbate generalized seizures in mesial temporal lobe epilepsy. Brain Res. *929*, 105–116.

Gaietta, G., Deerinck, T. J., Adams, S. R., Bouwer, J., Tour, O., Laird, D. W., Sosinsky, G. E., Tsien, R. Y., and Ellisman, M. H. (2002). Multicolor and electron microscopic imaging of connexin trafficking. Science *296*, 503–507.

Giepmans, B. N. (2004). Gap junctions and connexin-interacting proteins. Cardiovasc. Res. *62*, 233–245.

Giepmans, B. N., Hengeveld, T., Postma, F. R., and Moolenaar, W. H. (2001a). Interaction of c-Src with gap junction protein connexin-43. Role in the regulation of cell-cell communication. J. Biol. Chem. *276*, 8544–8549.

Giepmans, B. N., and Moolenaar, W. H. (1998). The gap junction protein connexin43 interacts with the second PDZ domain of the zona occludens-1 protein. Curr. Biol. *8*, 931–934.

Giepmans, B. N., Verlaan, I., and Moolenaar, W. H. (2001b). Connexin-43 interactions with ZO-1 and α- and β-tubulin. Cell Commun. Adhes. *8*, 219–223.

Goodenough, D. A., Goliger, J. A., and Paul, D. L. (1996). Connexins, connexons, and intercellular communication. Annu. Rev. Biochem. *65*, 475–502.

Goodenough, D. A., and Paul, D. L. (2003). Beyond the gap: functions of unpaired connexon channels. Nat. Rev. Mol. Cell. Biol. *4*, 285–294.

Green, C. R., Peters, N. S., Gourdie, R. G., Rothery, S., and Severs, N. J. (1993). Validation of immunohistochemical quantification in confocal scanning laser microscopy: a comparative assessment of gap junction size with confocal and ultrastructural techniques. J. Histochem. Cytochem. *41*, 1339–1349.

Hall, J. E., and Gourdie, R. G. (1995). Spatial organization of cardiac gap junctions can affect access resistance. Microsc. Res. Tech. *31*, 446–451.

Hare, J. F., and Taylor, K. (1991). Mechanisms of plasma membrane protein degradation: recycling proteins are degraded more rapidly than those confined to the cell surface. Proc. Natl. Acad. Sci. USA *88*, 5902–5906.

Hertig, C. M., Butz, S., Koch, S., Eppenberger-Eberhardt, M., Kemler, R., and Eppenberger, H. M. (1996). N-cadherin in adult rat cardiomyocytes in culture. II. Spatio-temporal appearance of proteins involved in cell-cell contact and communication. Formation of two distinct N-cadherin/catenin complexes. J. Cell Sci. *109*, 11–20.

Hunter, A. W., Jourdan, J., and Gourdie, R. G. (2003). Fusion of GFP to the carboxyl terminus of connexin43 increases gap junction size in HeLa cells. Cell Commun. Adhes. *10*, 211–214.

Itoh, M., Nagafuchi, A., Moroi, S., and Tsukita, S. (1997). Involvement of ZO-1 in cadherin-based cell adhesion through its direct binding to α catenin and actin filaments. J. Cell Biol. *138*, 181–192.

Jin, C., Lau, A. F., and Martyn, K. D. (2000). Identification of connexin-interacting proteins: application of the yeast two-hybrid screen. Methods *20*, 219–231.

Johnson, R. G., Meyer, R. A., Li, X. R., Preus, D. M., Tan, L., Grunenwald, H., Paulson, A. F., Laird, D. W., and Sheridan, J. D. (2002). Gap junctions assemble in the presence of cytoskeletal inhibitors, but enhanced assembly requires microtubules. Exp. Cell Res. *275*, 67–80.

Jordan, K., Solan, J. L., Dominguez, M., Sia, M., Hand, A., Lampe, P. D., and Laird, D. W. (1999). Trafficking, assembly, and function of a connexin43-green fluorescent protein chimera in live mammalian cells. Mol. Biol. Cell *10*, 2033–2050.

Kausalya, P. J., Reichert, M., and Hunziker, W. (2001). Connexin45 directly binds to ZO-1 and localizes to the tight junction region in epithelial MDCK cells. FEBS Lett. *505*, 92–96.

Laing, J. G., Chou, B. C., and Steinberg, T. H. (2005). ZO-1 alters the plasma membrane localization and function of Cx43 in osteoblastic cells. J. Cell Sci. *118*, 2167–2176.

Laing, J. G., Manley-Markowski, R. N., Koval, M., Civitelli, R., and Steinberg, T. H. (2001). Connexin45 interacts with zonula occludens-1 and connexin43 in osteoblastic cells. J. Biol. Chem. *276*, 23051–23055.

Laird, D. W., Castillo, M., and Kasprzak, L. (1995). Gap junction turnover, intracellular trafficking, and phosphorylation of connexin43 in brefeldin A-treated rat mammary tumor cells. J. Cell Biol. *131*, 1193–1203.

Laird, D. W., Jordan, K., and Shao, Q. (2001). Expression and imaging of connexin-GFP chimeras in live mammalian cells. Methods Mol. Biol. *154*, 135–142.

Laird, D. W., Puranam, K. L., and Revel, J. P. (1991). Turnover and phosphorylation dynamics of connexin43 gap junction protein in cultured cardiac myocytes. Biochem. J. *273*, 67–72.

Lauf, U., Giepmans, B. N., Lopez, P., Braconnot, S., Chen, S. C., and Falk, M. M. (2002). Dynamic trafficking and delivery of connexons to the plasma membrane and accretion to gap junctions in living cells. Proc. Natl. Acad. Sci. USA *99*, 10446–10451.

Lauf, U., Lopez, P., and Falk, M. M. (2001). Expression of fluorescently tagged connexins: a novel approach to rescue function of oligomeric DsRed-tagged proteins. FEBS Lett. *498*, 11–15.

Li, X., Olson, C., Lu, S., Kamasawa, N., Yasumura, T., Rash, J. E., and Nagy, J. I. (2004). Neuronal connexin36 association with zonula occludens-1 protein (ZO-1) in mouse brain and interaction with the first PDZ domain of ZO-1. Eur. J. Neurosci. *19*, 2132–2146.

Lindgren, M., Hallbrink, M., Prochiantz, A., and Langel, U. (2000). Cell-penetrating peptides. Trends Pharmacol. Sci. *21*, 99–103.

Liu, S., Taffet, S., Stoner, L., Delmar, M., Vallano, M. L., and Jalife, J. (1993). A structural basis for the unequal sensitivity of the major cardiac and liver gap junctions to intracellular acidification: the carboxyl tail length. Biophys. J. *64*, 1422–1433.

Lo, C. W. (2000). Role of gap junctions in cardiac conduction and development: insights from the connexin knockout mice *87*, 346–348.

Maza, J., Das Sarma, J., and Koval, M. (2005). Defining a minimal motif required to prevent connexin oligomerization in the endoplasmic reticulum. J. Biol. Chem. *280*, 21115–21121.

Meyer, R. A., Laird, D. W., Revel, J. P., and Johnson, R. G. (1992). Inhibition of gap junction and adherens junction assembly by connexin and A-CAM antibodies. J. Cell Biol. *119*, 179–189.

Musil, L. S., Cunningham, B. A., Edelman, G. M., and Goodenough, D. A. (1990). Differential phosphorylation of the gap junction protein connexin43 in junctional communication-competent and -deficient cell lines. J. Cell Biol. *111*, 2077–2088.

Musil, L. S., and Goodenough, D. A. (1991). Biochemical analysis of connexin43 intracellular transport, phosphorylation, and assembly into gap junctional plaques. J. Cell Biol. *115*, 1357–1374.

Musil, L. S., and Goodenough, D. A. (1993). Multisubunit assembly of an integral plasma membrane channel protein, gap junction connexin43, occurs after exit from the ER. Cell *74*, 1065–1077.

Musil, L. S., Le, A. C., VanSlyke, J. K., and Roberts, L. M. (2000). Regulation of connexin degradation as a mechanism to increase gap junction assembly and function. J. Biol. Chem. *275*, 25207–25215.

Nielsen, P. A., Baruch, A., Shestopalov, V. I., Giepmans, B. N., Dunia, I., Benedetti, E. L., and Kumar, N. M. (2003). Lens connexins α3Cx46 and α8Cx50 interact with zonula occludens protein-1 (ZO-1). Mol. Biol. Cell *14*, 2470–2481.

Nielsen, P. A., Beahm, D. L., Giepmans, B. N., Baruch, A., Hall, J. E., and Kumar, N. M. (2002). Molecular cloning, functional expression, and tissue distribution of a novel human gap junction-forming protein, connexin-31.9. Interaction with zona occludens protein-1. J. Biol. Chem. *277*, 38272–38283.

Ryeom, S. W., Paul, D., and Goodenough, D. A. (2000). Truncation mutants of the tight junction protein ZO-1 disrupt corneal epithelial cell morphology. Mol. Biol. Cell *11*, 1687–1696.

Saez, J. C., Berthoud, V. M., Branes, M. C., Martinez, A. D., and Beyer, E. C. (2003). Plasma membrane channels formed by connexins: their regulation and functions. Physiol. Rev. *83*, 1359–1400.

Sarma, J. D., Wang, F., and Koval, M. (2002). Targeted gap junction protein constructs reveal connexin-specific differences in oligomerization. J. Biol. Chem. *277*, 20911–20918.

Segretain, D., and Falk, M. M. (2004). Regulation of connexin biosynthesis, assembly, gap junction formation, and removal. Biochim. Biophys. Acta *1662*, 3–21.

Segretain, D., Fiorini, C., Decrouy, X., Defamie, N., Prat, J. R., and Pointis, G. (2004). A proposed role for ZO-1 in targeting connexin 43 gap junctions to the endocytic pathway. Biochimie *86*, 241–244.

Sepp, R., Severs, N. J., and Gourdie, R. G. (1996). Altered patterns of cardiac intercellular junction distribution in hypertrophic cardiomyopathy. Heart *76*, 412–417.

Severs, N. J., Dupont, E., Coppen, S. R., Halliday, D., Inett, E., Baylis, D., and Rothery, S. (2004). Remodelling of gap junctions and connexin expression in heart disease. Biochim. Biophys. Acta *1662*, 138–148.

Singh, D., Solan, J. L., Taffet, S. M., Javier, R., and Lampe, P. D. (2005). Connexin 43 interacts with zona occludens-1 and -2 proteins in a cell cycle stage-specific manner. J. Biol. Chem. *280*, 30416–30421.

Smith, J. H., Green, C. R., Peters, N. S., Rothery, S., and Severs, N. J. (1991). Altered patterns of gap junction distribution in ischemic heart disease. An immunohistochemical study of human myocardium using laser scanning confocal microscopy. Am. J. Pathol. *139*, 801–821.

Solan, J. L., Fry, M. D., TenBroek, E. M., and Lampe, P. D. (2003). Connexin43 phosphorylation at S368 is acute during S and G2/M and in response to protein kinase C activation. J. Cell Sci. *116*, 2203–2211.

Sorgen, P. L., Duffy, H. S., Sahoo, P., Coombs, W., Delmar, M., and Spray, D. C. (2004). Structural changes in the carboxyl terminus of the gap junction protein connexin43 indicates signaling between binding domains for c-Src and zonula occludens-1. J. Biol. Chem. *279*, 54695–54701.

Spach, M. S., Heidlage, J. F., Dolber, P. C., and Barr, R. C. (2000). Electrophysiological effects of remodeling cardiac gap junctions and cell size: experimental and model studies of normal cardiac growth. *86*, 302–311.

Stevenson, B. R., Siliciano, J. D., Mooseker, M. S., and Goodenough, D. A. (1986). Identification of ZO-1, a high molecular weight polypeptide associated with the tight junction (zonula occludens) in a variety of epithelia. J. Cell Biol. *103*, 755–766.

Toyofuku, T., Akamatsu, Y., Zhang, H., Kuzuya, T., Tada, M., and Hori, M. (2001). c-Src regulates the interaction between connexin-43 and ZO-1 in cardiac myocytes. J. Biol. Chem. *276*, 1780–1788.

Toyofuku, T., Yabuki, M., Otsu, K., Kuzuya, T., Hori, M., and Tada, M. (1998). Direct association of the gap junction protein connexin-43 with ZO-1 in cardiac myocytes. J. Biol. Chem. *273*, 12725–12731.

Umeda, K., Matsui, T., Nakayama, M., Furuse, K., Sasaki, H., Furuse, M., and Tsukita, S. (2004). Establishment and characterization of cultured epithelial cells lacking expression of ZO-1. J. Biol. Chem. *279*, 44785–44794.

VanSlyke, J. K., and Musil, L. S. (2000). Analysis of connexin intracellular transport and assembly. Methods *20*, 156–164.

Wei, C. J., Francis, R., Xu, X., and Lo, C. W. (2005). Connexin43 associated with an N-cadherin-containing multiprotein complex is required for gap junction formation in NIH3T3 cells. J. Biol. Chem. *280*, 19925–19936.

Willecke, K., Eiberger, J., Degen, J., Eckardt, D., Romualdi, A., Guldenagel, M., Deutsch, U., and Sohl, G. (2002). Structural and functional diversity of connexin genes in the mouse and human genome. Biol. Chem. *383*, 725–737.

Zhu, C., Barker, R. J., Hunter, A. W., Zhang, Y., Jourdan, J., and Gourdie, R. G. (2005). Quantitative analysis of ZO-1 colocalization with Cx43 gap junction plaques in cultures of rat neonatal cardiomyocytes. Microsc. Microanal. *11*, 244–248.